Enhanced idealized explicit FEM for predicting welding deformation in complex large-scaled structure and application to the real structure

Enhanced idealized explicit FEM for predicting welding deformation in complex large-scaled structure and application to the real structure

IKUSHIMA Kazuki*, MAEDA Shintaro**, IESHITA Teruya***, KAWAHARA Atsushi*, ABE Yuuta****, KIUCHI Hirotaka**** and SHIBAHARA Masakazu*

(*Member, Graduate School of Engineering, Osaka Prefecture University
**Student Member, Graduate School of Engineering, Osaka University,
***Student Member, Graduate School of Engineering, Osaka Prefecture University
**** Member, Hitachi Construction Machinery)

In the fabrication of steel structures, welding is widely utilized to join the materials. Due to the welding, distortions are inevitably generated, and these distortions may cause problems in accuracy or labor costs. In this research, to establish an analysis method which can predict the welding distortions in complex large-scale structures, we proposed a new analysis method based on the Idealized Explicit FEM. In the proposed method, an algebraic multigrid method was introduced to the Idealized Explicit FEM to achieve an efficient analysis in realistic structures. The proposed method was applied to the prediction of the welding distortion in the base structures of the construction machine. The number of welding passes was 28. The predicted and measured distortions were compared. As a result, it was demonstrated that the proposed method has a high analysis accuracy. The analysis finished within the realistic time within 35 hours. The influence of welding sequence on the deformation was also investigated by changing welding sequence. The result indicated that the welding sequence may have considerable effect on the welding distortion and is necessary to be investigated in advance of the production.

1. Introduction

Welding deformation may become problematic in structural fabrication. In particular in the construction of complex structures with multiple members, gaps and linear misalignments occur due to deformation associated with welding and this may be the cause of errors and decrease in dimensional accuracy in the succeeding assembly process. Due to this, there is an increase in human labour cost and operational time to correct welding deformation. Also, since the quality and reliability of products are all affected by the occurrence of welding deformation, it is desirable that a method of prior investigation of welding deformation using numerical simulation should be established.

It is possible to analysis welding deformation in structures by carrying out non-linear finite element analysis[1] based on thermal elastic plastic theory and there are many existing examples of prediction of welding and residual stress in welded joints[2-5]. However, since processing time and memory usage increases proportionate to the square - cube of the analytical scale when a static implicit method FEM using a direct method including LU decomposition is used to solve the global stiffness equations used in commercial finite element structural analysis software, as the structure becomes larger so the calculation

resources used for the analysis increases extremely. In addition, since welding problems involve the problem of strong non-linearity due to localized melting in the vicinity of the torch caused by the heat input from the welding torch, there is a requirement for a detailed analysis and since the calculation scale is greater than for ordinary structural analyses, the question of calculation scale is a major difficulty for the performance of welding thermal elastic plastic analysis on actual large structures.

Thus, since analysis scale is a problem for FEM thermal elastic plastic analysis of welding, there have been many studies on increasing efficiency of analytical methods. Studies of increasing the speed of FEM thermal elastic plastic analysis include the adaptive mesh method of Boitout et al[6], which embeds the refined mesh solid element in the entire solid model which expresses the welding heat source vicinity, the composite mesh model of Goldak et al[7] which embeds a mesh of the welding heat source vicinity into a mesh of the whole structure, and the dynamic substructuring method of Brown et al[8] in which the weldment is subdivided from the overall structure and further subdivided as the welding heat source is moved. Also, in these methods the total structure and weldment heat source vicinity are analysed separately, but Murakawa et al have developed an iterative substructure method (ISM)[9] which increases analysis speed by defining the total structure as a weakly non-linear domain and repeating the analysis of the strongly non-linear domain of the weldment vicinity and used this in comparatively large-scale analyses[10]. However, all of these methods are based on static implicit FEM in which the direct method of solving the complete stiffness equations is used and since, in the analysis of actual large-scale structures, both the computational time and memory usage increase as the analysis scale increases, analysis becomes extremely difficult.

Accordingly, the present study is of enhancement of idealized explicit FEM[11] developed by the present authors to solve the problems of analysis scale used in FEM thermal elastic plastic analysis to predict welding deformations in the analysis of actual large-scale structures. Since, in the analysis of actual large-scale structures, it is necessary to make an efficient analysis of the complex structural deformations, it is an aim of the present study to achieve a significant increase in analysis speed by the introduction of a multigrid method[12] into the idealized explicit FEM. Furthermore, the validity of the analysis results found by the proposed method is proved through a comparison of the results of analysis by the proposed method and experimental results and its utility in the analysis of actual large-scale structures was investigated. In addition, there was also an investigation of the effects of the welding sequence on welding deformation during the welding of building structures.

2. Increasing the efficiency of idealized explicit FEM in the analysis of real large-scale structures

2.1 Summary of idealized explicit FEM

Idealized explicit FEM is an analytical method which makes it possible to increase the speed and reduce the memory usage of structural analysis based on dynamic explicit FEM. A summary of the analytical theory is described below.

In idealized explicit FEM, analysis proceeds in the sequence ①, ② and ③ shown below. ① The load increment, that is, the temperature increment in the welding transient state is loaded and this state is maintained ② Displacement is calculated until it reaches a static equilibrium state by using Basic Equation (1) of dynamic explicit FEM ③ When a static equilibrium state is achieved, the sequence returns to Step ① in order to move on to the calculation of the next load step.

$$\left(\frac{1}{\Delta t^2}[M] + \frac{1}{2\Delta t}[C]\right)\{U\}_{t+\Delta t} =$$

$$\{F\}_t - \sum_{e=1}^{Ne}\int_{Ve}[B]^T\{\sigma\}\,dV + \frac{2}{\Delta t^2}[M]\{U\}_t$$

$$-\left(\frac{1}{\Delta t^2}[M] - \frac{1}{2\Delta t}[C]\right)\{U\}_{t-\Delta t} \qquad (1)$$

Here, $[M]$, $[C]$, $[B]$ and $\{\sigma\}$ are, respectively, mass matrix, damping matrix, displacement-strain relationship matrix and stress vector and $\{U\}_{t+\Delta t}$, $\{U\}_t$, $\{U\}_{t-\Delta t}$ and $\{F\}_t$ are, respectively, the displacement vectors at time $t+\Delta t$, t and $t-\Delta t$ and the load vector at time t. Also, N_e is the number of elements in the analysis model and V^e is the volume of the elements.

Here, by using the mass matrix $[M]$ and damping matrix $[C]$ for a node concentrated-type diagonal matrix, the matrix operation shown in Equation (1) is no longer a simultaneous equation and less memory may be used for performance of the analysis. Also, the number of time steps required to obtain static equilibrium above is reduced by using the mass matrix $[M]$, shown below, in the process ② and ③ above.

$$\rho_i = \frac{\Delta t_{cr}^2\,E}{\Delta l_i^2} \qquad (2)$$

$$[M_e] = \int_{Ve}\{\rho_i\}[N]^T[N]dV \qquad (3)$$

Here, E is Young's modulus, Δl_i is the element length of each of the directions and Δt_{cr} is the critical time increment per 1 step. The mass matrix $[M_e]$ per element unit is determined by the Equation (3) integral. $[N]$ is the shape function of the elements. Since, by using the mass matrix thus derived, the critical value for the time increments can be uniform, whatever the element size or material constant, it is possible to reduce the number of the time steps required to converge on static equilibrium. In order that the analysis should progress stable, Δ_t in Equation (1), which finds the displacement in the time step, must be set to be smaller than the critical time increment $\Delta t_{cr.}$ In the present study, Δt and Δt_{cr} are, respectively, 0.7 and 1.0.

The damping matrix [C] is defined using Equations (4) and (5), based on critical damping in a one-dimensional vibration problem and using the diagonal component k_{ii} in the stiffness matrix $[K]$ and the diagonal component m_{ii} in the mass matrix $[M]$.

$$c_{ii} = 2\sqrt{m_{ii}k_{ii}} \tag{4}$$

$$[C] = \begin{bmatrix} c_{11} & \cdots & 0 & \cdots & 0 \\ & \ddots & \vdots & & \vdots \\ & & c_{ii} & \cdots & 0 \\ & & & \ddots & \vdots \\ Sym. & & & & c_{nn} \end{bmatrix} \tag{5}$$

As described above, since, in the present method when solving the non-linear global stiffness equation formulated based on static implicit FEM, static equilibrium is found by a pseudo-dynamic solution, it may be described as being similar to a dynamic relaxation method[13]. Also in the present method, pseudo-dynamic analysis is performed to obtain a convergence solution until the dynamic terms no longer have any effect and, since inertia terms and damping terms have no effect when the convergence solution is obtained, it is possible to use a mass matrix and damping matrix to reduce the number of steps required to reach convergence. In the present method, as described above, adjustment of time increments equivalent to the mass scaling[14] performed in dynamic explicit FEM is carried out by virtual scaling of the density of the elements based on the Courant condition in each element. Due to this, there is a reduction in the differences in the critical time increments for each of the elements due to the extreme differences between the Young's modulus in the high-temperature region near the torch and in other regions, which are particularly problematic in analysis of welding. By using this method, idealized explicit FEM can achieve a large reduction in the calculation time of welding mechanical analysis compared to static implicit

FEM[11,23]. Also, as when CG or other iterative method is used, it is possible to carry out an analysis with a memory consumption that is proportional to the number of elements.

2.2 The multigrid method

In numerical simulation, it is very often necessary to solve large-scale simultaneous equations. In the multigrid method, one method of efficiently solving large-scale simultaneous equations, long-wavelength errors in iterative solutions are converged by a coarse grid and short-wavelength errors are converged by a fine grid. Since by adopting this kind of method, long-wavelength errors, which slowly converge in conventional iterative methods, can converged more quickly, it is expected to be a method of solving simultaneous equations at high speed in large-scale problems. It has also been demonstrated that the computation required to obtain solutions with constant accuracy is proportional to the degree of freedom and it is known to be a high-speed iterative solution[15,16]. Thus the multigrid method has attracted attention as a useful solution method and is currently a method which is being widely developed.

However, in multigrid method calculations, it is necessary to prepare a coarse grid to converge errors related to the long-wavelength components and multigrid method is often used in finite differences method since it is easy to prepare coarse grids. Since, in unstructured grids with a complex structure such as FEM, the cost of mesh preparation is large and preparation of coarse grids is difficult, it is difficult to use the multigrid method for FEM.

The algebraic multigrid (AMG) has been proposed as a method to solve this problem[17-19]. With the AMG, a coarse grid is prepared solely from the algebraic properties of the coefficient matrix of simultaneous equations, and the multigrid approach is used for the grid. Since, when this method is used, coarse grids are prepared automatically by AMG and there is no necessity for a coarse grid to be prepared by the user, it has attracted attention as a rapid and universal solution method and a range of methods have been developed. The main solution methods that use AMG include the method of Stüben[20], the method of Brandt et al[21] and methods using smoothed aggregation[22]. In these methods, when interpolation is performed from higher levels to lower levels, only the sequence of matrix creation is different so that when an interpolation matrix is created, the interpolation $[P_i]$ is found such that the vector $\{e\}$, which satisfies the following equation, closely approximates on the different levels.

$$[K_i]\,\{e\} \approx 0 \qquad\qquad\qquad (6)$$

In Equation (6), $[K_i]$ is the coefficient matrix on the ith level and $\{e\} \neq 0$. Since $\{e\}$

satisfying Equation (6) corresponds to a long-wavelength error and is a component which is difficult to converge with a fine grid using the iterative method, the solution is found efficiently by correcting such components with a lower level grid.

The lower level stiffness matrix, i.e. coefficient matrix $[K_{i+1}]$, is calculated by the following equation based on the interpolation matrix $[P_{i+1}]$ and upper-level coefficient matrix $[K_i]$.

$$[K_{i+1}] = [P_{i+1}]^T [K_i] [P_{i+1}] \qquad (7)$$

Of the three representative AMG methods noted above, in the method of Stüben and the method of Brandt et al it is necessary to choose the degree of freedom from the upper level grids to retain in the lower level. In addition, in order to prepare a lower level coefficient matrix in these methods, it is necessary to adjust multiple parameters. With the smoothed aggregation, on the other hand, as shown in Fig. 1, the lower level degree of freedom is expressed as an aggregate of the upper level degrees of freedom (DOFs). When this is done, a judgement is made that, based on the relative strength of the relationship between the DOFs described by the coefficient matrix, the upper level DOFs are always to be in one of the lower level aggregates.

It is thus possible to introduce the multigrid method into the FEM by using an AMG method and since one such method, the smoothed aggregation method involves few tuning parameters and is considered easy to use, the solutions proposed henceforward in this study for the welding deformation analysis of large-scale complex structures will be based on this method.

2.3 Idealized explicit FEM incorporating the multigrid method

In FEM welding thermal elastic plastic analysis, in order to perform consecutive analysis of welding phenomena, a welding mechanical phenomenon is split into load steps from the start of heating to complete cooling and elastic plastic non-linear analysis is carried out in each of the load steps. The number of load steps in the entire analysis extends from several thousands to several tens of thousands and since processing of the multigrid method described in the previous section includes complicated computational procedures, it is extremely inefficient to carry out these processes in all of the load steps. Accordingly, in the present study, with the method shown as the flow in Fig. 2, the multigrid method was introduced into idealized explicit FEM. First aggregates are prepared as analysis pre-processes[20], LU decomposition performed and stored in the lowest level grid. Next, the temperature field is renewed and a global stiffness matrix is prepared in the renewed temperature field. Here, a stiffness matrix is prepared only on the highest level. This is

because, since non-linear deformation due to temperature changes accompanying welding progress is localized deformation, occurring in a narrow region in the vicinity of the torch, tracking of non-linear deformation is enhanced by renewal of the stiffness matrix on the highest, that is, input mesh. Also, memory usage is reduced in proportion to the analysis degree of freedom, by the stiffness matrix of each of the levels being stored in a sparse matrix format.

Displacement is calculated on the basis of the idealized explicit FEM approach, using the renewed highest-level stiffness matrix and the stiffness matrices on other levels. This is carried out following the procedures shown in Fig. 3. First, in the first-level grid, displacement is calculated by performing the idealized explicit procedures for several time steps for a given residual force vector, the residual force vector in this state being calculated by the following equation.

$$\{R_1\} = \{F_1\} - [K_1]\{U_1\} \tag{8}$$

The residual force vector $\{R_1\}$ thus calculated is interpolated on the second-level grid using the following equation and the load vector $\{F_2\}$ on the second-level grid is calculated.

$$\{F_2\} = [P_2]^T\{R_1\} \tag{9}$$

Here, $[P_2]$ expresses the interpolation function generated when the second-level grid is prepared. The method used to prepare the interpolation function is a method in which a pseudo-Laplacian is used, described in the literature[20] which refers to strongly anisotropic problems. Displacement is calculated on the basis of the idealized explicit method as in the case of the first level, using the load vector obtained by the interpolation process expressed in Equation (9). The above process is performed recursively until the lowest grid is reached and the lowest grid displacement is calculated by the direct method using the LU decomposition calculated at the time when the grid was prepared.

After displacement is calculated at the lowest level, the lowest level displacement is interpolated onto the third-level grid, the sum of this with the displacement in the third-level grid is found and the third-level displacement is thus renewed.

$$\{U_3\} \leftarrow \{U_3\} + [P_4]\{U_4\} \tag{10}$$

Displacement is calculated based on the idealized explicit method using the third-layer grid displacement thus calculated and the load vector. After the displacement calculation is completed by idealized explicit method, the third-level displacement vector is interpolated into the second level and displacement is calculated in the same way as in the third level. These processes are performed recursively up to the highest grid and a single iterative computation by the multigrid method is finished. For convenience of explanation, four levels

are described but in actual analyses, coarse grids are created recursively until at least the fixed number of analysis DOFs included in a level is reached.

Furthermore, in conventional multigrid methods, a stationary iteration method such as the Jacobi method is frequently used in the calculation part as in Fig. 3 but idealized explicit FEM was used in this study. This is because since a stationary iteration method such as the Gauss-Seidel method or SOR method involves sequential processing, parallelisation is difficult. Parallelisation can be easily applied to the Jacobi method but since a condition required for convergence with the Jacobi method is that the coefficient matrix is strict diagonal dominant, it is highly possible that convergence cannot be obtained stably and it is unused for reasons of stability of analysis.

The displacement in a single load step is found by repeating the above computational procedure until the specified convergence conditions are satisfied. Also, calculation of the load steps is repeated, and analysis is progressed, until cooling is completed. Also, the above computational procedure is implemented by expanding the idealized explicit FEM[23] using GPU parallelisation previously developed by the present authors and, since there is LU decomposition, for which GPU parallelisation is not appropriate, only in the lowest level operations, a conventional CPU was used.

By using this computational procedure, the proposed method should be able to achieve computational accuracy and convergency in the analysis of thin plate structures superior to conventional idealized explicit FEM.

3. Prediction of welding deformation during assembly processes of real large structures

3.1 Analytical model and analytical conditions

The analytical method proposed in the previous section was applied to the prediction of welding deformation during assembly processes of real large structures and the analytical accuracy along with the tendencies of welding deformation in real large structures both investigated.

The analysis object was a structure shown in Fig. 4 modelling the base of a construction machine. The overall dimensions were a length of 4m, width of 2m and height of 0.5m. The number of elements and number of nodes resulting from the mesh division of the structure were, respectively, 502,308 and 608,394. The main frame, tail frame and side frame were fabricated separately, the main frame and tail frame were welded first and then the side frame was joined. In this analysis, a total of 28 passes of welding were analysed, as shown in Fig. 5. The welding conditions for each welding pass are shown in Table 1. Of these welding passes, from Pass 1 to Pass 4 (Stage 1) and from Pass 23 to pass 28 (Stage III) were, respectively,

welding of the main frame and tail frame and finishing welding and welding was performed manually. The other passes, from Pass 5 to Pass 22 (Stage II) are the welding of the main frame and side frame, for which automatic welding by robot was used. Before this welding, tack welding was performed on the main frame and side frame and on the tail frame but deformation during tacking was not taken into consideration in this study. Also, the stiffness of the locations where welding was performed were modelled by only those elements corresponding to the tacks and fillets. There was no constraint during the welding in Stage 1, from Pass 1 to Pass 4, and the constraint conditions from Pass 5 to Pass 22 (Stage II) and from Pass 23 to Pass 28 (Stage III) during the welding were complete constraint of, respectively, the locations shown in Fig. 6 (a) and (b). The welding method for both manual and automatic welding was GMA welding. The material for the model was SM490A, with the assumption of temperature dependency of the material properties shown in Fig. 7[24]. In the analysis, a volumetric heating model was employed in which the elements in a rectangular region, with the longer dimension being the direction of torch travel, being heated uniformly. An element birth and death method[25] is used in which the elements corresponding to the weld metal are in a deactivated state when welding starts and when, during welding, the torch reaches the weld metal that has been deactivated, the elements are activated. The results of heat conduction analysis showed that there were a total of 53,720 temperature steps in the 28 passes.

Thermal elastic plastic analysis was carried out by the proposed method using the above conditions. A computer, fitted with an Intel Core i7 3.4GHz CPU, 64GB memory and an NVIDIA GeForce RTX 2080Ti as the GPU, was used for the analysis.

3.2 Welding deformation analysis results

Fig. 8 shows the analysis results for welding deformation after the initial welding, from Pass 1 to Pass 4 (Stage 1). The figure shows displacement distribution in the z direction, with a deformation magnification ratio of 100-fold. The shape before welding is shown by the thin black line. It is clear from Fig. 8 as welding progresses from Pass 1 to Pass 4, deformation occurs so that the tail frame falls in the negative direction along the z axis. As is clear from Fig. 5 (b) and (c), this is because, since the welding line up to Pass 4 is located on the lower side of the neutral plane as the weldment contracts, the tail frame deforms so that it rotates clockwise around the y axis.

Fig. 9 shows a comparison of the deformation before and after Pass 14 and Pass 17 welding during automatic welding by robot. Pass 14 and Pass 17 locate respectively on the bottom surface and upper surface of the side frame and both have relatively long weld length.

The deformation magnification ratio in Fig. 9 is 50. It is clear from this that the deformation associated with Pass 17 was greater than that at Pass 14. The reason for can be assumed that, when Pass 14 welding was carried out, the 23rd pass of welding had not been carried out on the lower surface of the side frame so that the stiffness between the side frame and main frame was small and the deformation at Pass welding 14, when the lower surface wall was welded, is limited to localized deformation. In the case of Pass 17, when the upper surface is welded, on the other hand, since Pass 8 and Pass 16 have been completed, stiffness of the weldment vicinity is strong and this acts as a constraint with the result that a large shrinkage plastic strain is created in the weldment and the entire side frame deforms.

Fig. 10 shows the displacement distribution in z direction after completion of robot welding. As this figure shows, when robot welding has been completed, from Pass 17 of welding as shown in Fig. 9(d), it is clear that the end of the side frame in the y axis direction deforms so that it is lifted and directed upwards. Since, in welding after Pass 17, there are multiple locations, as in Passes 18, 20 and 21 and shown in Fig. 6(a) and (b), where the upper surface of the side frame and the main frame are joined, the side frame is lifted with the transverse shrinkage during these passes. Fig. 11 shows the displacement distribution in the z direction after all the welding passes. It is clear from this figure that, with the final finishing weld, although deformation occurs at sections close to the welded parts of the side frame, there is no great change in the welding deformation throughout the entire side frame.

Next, the base of the machine was investigated. Since the base of the machine rotates on the drive part, it is mounted on a bearing and, since deformation of the base is linked to the performance as the bearing slides, the base, particularly the dimensional accuracy in the out-of-plane direction of the back surface of the main frame, is important. Fig. 12 shows a comparison between measurements and analysis results for displacement distribution in the z direction on the back surface of the main frame. For measurement of the deformation, a triangular shape as a reference surface was prepared from three-dimensional coordinate values, measured using FARO[26], a three-dimensional coordinate value measurement system, and the perpendicular distances between the reference surface to the coordinate values were measured as the amount of deformation. As shown in Fig. 12(a), the three-dimensional coordinate values are measured in a matrix form from 1 to 16 in x direction and from A to N in y direction. It is clear from Fig. 12 that the tendency of the distribution of deformation in the analysis results and measurement results agree well. Also, Fig. 13 shows a comparison of z direction displacement distribution in the analysis results and measurement results on the

2B-3B line and on the 13B-13L line, as defined in Fig. 12(a). It is clear from Fig. 13 that both of these agree well for amount of deformation and that the analysis has very high accuracy.

The calculation time required for this analysis was 35 hours and it can be said that welding distortion in a real structure can be analysed with high accuracy in a practical computing time, by using the proposed method.

4. Influence of welding sequence on weld deformation

4.1 Setting the welding sequence

Since an operator's seat and other parts are to be fitted into the side frame in the machine structure that was the object of analysis in the previous section, the deformation of the side frame during welding is important for reasons of assembly precision. Accordingly, the relationship between the amount of welding deformation and welding sequence was investigated using the proposed method with the aim of reducing the weld deformation occurring in the side frame.

The welding sequence is such that manual welding is used from Pass 1 to Pass 4 (Stage 1) and from Pass 23 to Pass 28 (Stage III), and it is difficult to alter the welding sequence for these stages for reasons of constraining jigs and the welding position. Because of this, the welding from Pass 5 to Pass 22, which is carried out by robot welding, is investigated here.

As shown in Fig 9(d) and Fig 10, and described in the previous section, in the welding from Pass 18 to Pass 22 (Stage II), it can be assumed that the side frame is lifted up from the main frame due to transverse shrinkage of the upper surface of the side frame during the passes when the side frame and main frame are joined. Accordingly, for the welding sequence from Pass 18, the welding was first completed at Pass 18, Pass 20 and Pass 21, where there is this possibility that the side frame may lift due to transverse shrinkage. The aim was to reduce the stiffness during these welding passes and thus to reduce the transverse shrinkage produced with the result that the lift of the side frame is minimized. Table 2 shows the modified welding sequence, with the assumption that Passes 18, 20 and 21 are prioritized. In this particular sequence, however, welding is carried out at Pass 20, the 5th welding pass after the start of robot welding starts, and then welding Pass 21 and Pass 18 are performed. Subsequent welding was performed without interruption in the sequence before the change, and this is defined as the welding sequence which focusses on transverse shrinkage.

It was also noted in the previous section that, in the case of welding deformation at Pass 14 and Pass 17, as shown in Fig. 9, when the weld line in each of these passes was long and welding had also been performed previously in the vicinity of these passes, there is a

possibility that welding deformation became larger. Accordingly, investigation focusing on weld length and welding sequence was performed. Fig. 14 shows the size of the weld length at each pass. As shown in the figure, with the welding sequence analysed in the previous section, the passes with a comparatively short weld line are performed in the first half and those with a long weld line in the second half. Accordingly, a welding sequence was considered, as in Fig. 15, in which welding deformation is reduced by passes with long weld length being welded at the stage where welding had not been performed nearby. This figure shows the welding lengths in the welding sequence after the change when Pass 17, where the weld line was longest in the welding sequence before the change, is set as the fifth pass after the start of automatic welding and subsequently the pass sequence is set such that the weld length becomes shorter in order up to Pass 22, where the automatic welding ends. This welding sequence is referred to as the welding sequence focusing on weld length.

Welding deformation analysis was performed with these two conditions set and the influence of the welding sequence on deformation investigated.

4.2 Analysis results

Fig. 16 shows the displacement distribution in the z direction when the welding sequence focusing on transverse shrinkage is set. The analysis results shown in the figure take the deformation produced by manual welding both before and after automatic welding into consideration. In the method of representing the deformation the magnification ratio was 50, as in Fig. 9. It is clear from Figs. 11 and 16 that it is possible to reduce the welding deformation that lifts the side frame through the use of the welding sequence focusing on transverse shrinkage. Similarly, Fig. 17 shows the displacement in the z direction when the welding sequence focusing on weld length is set. From this figure and Fig. 11, it can also be confirmed that in the welding sequence that focuses on weld length, the side frame lifts less than in the original welding sequence.

Fig. 18(a) and (b) show a comparison of the displacement in the z direction on the c-a line and a-b line shown in Fig. 4. In these figures, the blue circular symbols   , green square symbols   and red diamond symbols   are, respectively, the displacement in the z direction with the original welding sequence, with the welding sequence focusing on transverse shrinkage and with the welding sequence focusing on weld length. It is clear from these figures that, when the welding sequence focusing on transverse shrinkage is set, the z direction displacement over almost the entire c-a line and a-b line can be reduced more than with the original welding sequence and in the vicinity of point b there was only a small increase in the z direction displacement compared to the original sequence. With the welding

sequence focusing on weld length, on the other hand, deformation is less than with the original sequence over the entire c-a line and a-b line so that it can be said that the deformation reduction effect is greater than with the welding sequence focusing on transverse shrinkage. Thus, with the structure analysed in this study, it is clear that welding sequence has a large effect on welding deformation. Since it is possible that, depending on the stiffness and constraint of the structure during welding, the welding sequence may influence welding deformation, it is preferable that the effects of welding deformation and welding sequence should be investigated beforehand.

As shown in this section, welding deformation analysis of complex real structures was performed rapidly through the use of an idealized explicit FEM incorporating the algebraic multigrid method proposed in this study. Furthermore, since it was possible to investigate the effects of welding sequence in a practical computation time by using the proposed rapid analysis method, it is expected that this will be used in the investigation of welding deformation in a range of structures.

5. Conclusion

In this study, a novel idealized explicit FEM incorporating an algebraic multigrid method was proposed to make possible a numerical analysis of welding deformation in real large structures. In order to show the utility of the proposed method, it was used for the prediction of welding deformation when the main frame, tail frame and side frame of the base of a construction machine are welded and the computation time and analysis accuracy were investigated. The following findings were made as a result of an investigation using the proposed method of the influence of the welding sequence on welding deformation when the mechanical structure was welded.

1) As a result of the use of the proposed method for analysis of weld deformation of a construction machine, it was possible to perform thermal elastic plastic analysis of 28 passes in a 600,000-node analytical model analysis in 35 hours using a single commercially available computer and it was shown to be possible to conduct an analysis of welding deformation when an real large structure is assembled in a practical computation time by using the proposed method.

2) A comparison was made of the results of measurement of welding deformation in the base plate of a construction machine base using a FARO contact-type three-dimensional coordinate measurement device and the results of welding deformation analysis using the proposed method. As a result, it was confirmed that, since the

welding deformation predicted by this analysis was a good agreement with the deformation measured using FARO, the proposed method has good analysis accuracy for welding deformation.

3) In order to show the utility of the proposed method in the investigation of welding deformation in real large structures, an investigation was made of the changes in welding deformation when the welding sequence was changed using the proposed method. In this investigation, welding sequences focusing on weld length and transverse shrinkage were set for analyses of welding deformation. As a result, it was clear that when the welding sequence was changed, there was an evident difference in welding deformation. These results give some indication of the influence of welding sequence on welding deformation and it will be necessary for this to be investigated further in the future.

4) In the present study, since it was possible to achieve a large reduction in the computation time required for analysis of welding deformation in complex structures by using the proposed idealized explicit FEM incorporating an algebraic multigrid method, it was possible to investigate the welding sequence in complex structures. It is expected that from now this will be of utility in the analysis of welding deformation in a wide variety of large structures.

References

1) Y. Ueda, T. Yamagawa: Analysis of thermal elastic plastic behaviour of metals during welding by the finite element method, Journal of the JWS, Vol.42, No.6 (1973), pp.567-577.
2) T. Terasaki, D. Yamagawa, S. Tonai: Study on accurate numerical analysis of welding residual stress and welding deformation generated in bead-on-plate, Journal of the Society of Naval Architects of Japan Vol.191 (2002), pp.239-245.
3) M. Mochizuki, M. Hayashi, T. Hattori: Effect of welding sequence on residual stress in multi-pass butt-welded pipe joints, Transactions of the Japan Society of Mechanical Engineers. A, Vol.62, No.604 (1996), pp.2719-2725.
4) A. H. Yaghi, T. H. Hyde, A. A. Becker, W. Sun, G. Hilson, S. Simandjuntak, P. E. J. Flewitt, M. J. Pavier, D. J. Smith: A Comparison Between Measured and Modeled Residual Stresses in a Circumferentially Butt-Welded P91 Steel Pipe, Journal of Pressure Vessel Technology, Vol.132, No.1 (2010), 011206.
5) D. Deng, S. Kiyoshima: FEM Prediction of Welding Residual Stresses in a SUS304 Girth-Welded Pipe with Emphasis on Stress Distribution Near Weld Start/End Location, Computational Materials Science, Vol.50 (2010), pp.612-621.
6) F. Boitout, J. Bergheau: The Numerical Simulation of Welding in Europe: Present Capabilities and Future Trends, Trans. JWRI, Vol.32, No.1 (2003), pp.197-204.
7) J. Goldak, M. Mocanita, V. Aldea, J. Zhou, D. Downey, D. Dorling : Predicting Burn-

through When Welding on Pressurized Natural Gas Pipelines, Proceedings of 2000 ASME Pressure Vessels and Piping Conference, (2000), pp.23-27.

8) S. B. Brown, H. Song: Rezoning and Dynamic Substructuring Techniques in FEM Simulations of Welding Processes, ASME Journal of Engineering for Industry, Vol.155 (1993), pp.415-423.

9) H. Murakawa, I. Oda, S. Ito, H. Serizawa, M. Shibahara, H. Nishikawa: Iterative substructure method for fast computation of thermal elastic plastic welding problems, Journal of the Kansai Society of Naval Architects, No.243 (2005), pp.67-70.

10) H. Nishikawa, H. Serizawa, H. Murakawa: Actual application of large-scaled FEM for analysis of mechanical problems in welding, Quarterly Journal of the JWS, Vol.24, No.2 (2006), pp.168-173.

11) M. Shibahara, K. Ikishima, S. Ito, K. Masaoka: Computational method for transient welding deformation and stress for large scale structure based on dynamic explicit FEM, Quarterly Journal of the JWS, Vol.29, No.1 (2011), pp.1-9.

12) A. Brandt: Multi-Level Adaptive Solutions to Boundary-Value Problems, Mathematics of Computation, Vol.31, No.138 (1977), pp.333-390.

13) M. Tsuda, I. Hagiwara: Dynamic-explicit finite element analysis methods for large-deformation quasi-static problems : 1st report, presentation of research theme, Transactions of the Japan Society of Mechanical Engineers. A, Vol.64, No.622 (1998), pp.114-121.

14) E. Kurosawa, C. Nakagawa: High-efficiency coupled solidification-thermal stress simulation of casting based on explicit finite element method, Transactions of the Japan Society of Mechanical Engineers, Vol.81, No.827 (2015), p.15-00192.

15) K. Karatani, Y. Okuda, M. Yagawa, A. Kreschel, K. Stuben: Performance evaluation of AMG (Algebraic Multigrid) solver for large-scaled FEM analysis, Transactions of JSCES, Vol.2001 (2001), p.20010022.

16) C. Arakawa: Numerical Hydraulic Engineering Tokyo University Press (1994), Chapter 9.

17) K. Stuben and U. Trottenberg: Multigrid Methods: Fundamental Algorithms, Model Problem Analysis and Applications, Lecture Notes in Mathematics, Vol.960 (1982), pp.1-176.

18) J. W. Ruge and K. Stuben: Efficient Solution of Finite Difference and Finite Element Equations by Algebraic Multigrid, The Institute of Mathematics and its Applications Conference Series, Clarendon Press, Oxford, (1985), pp.169-221.

19) J. W. Ruge and K. Stuben: Algebraic multigrid (AMG) in Multigrid Methods, Frontiers in Applied Mathematics, S. F. McCormick ed., SIAM (1987), pp.73-130.

20) T. Füllenbach and K. Stüben: Algebraic multigrid for selected PDE systems, Proceedings of the 4th European Conference, Elliptic and Parabolic Problems (2002), pp.399-410.

21) A. Brandt, S. McComick and J. Ruge: Algebraic multigrid (AMG) for sparse matrix equations, Sparsity and its Applications, Cambridge University Press (1984), pp.257-284.

22) M. W. Gee, J. J. Hu and R. S. Tuminaro: A new smoothed aggregation multigrid method for anisotropic problems, Numerical Linear Algebra with Applications, Vol.16 (2009),

pp.19-37.

23) K. Ikishima, S. Ito, M. Shibahara: Development of parallelized Idealized Explicit FEM using GPU, Quarterly Journal the JWS, Vol.31, No.1 (2013), pp.23-32.

24) Japan Nuclear Energy Safety Organization: Project of integrity assessment of flawed components with structural discontinuity (IAF) material properties data book at high temperature for dissimilar metal welding in reactor pressure vessel (2013), pp.A1-120-A1-128.

25) T. Harada, K. Ikushima, M. Shibahara, F. Kimura, T. Morimoto: Study on Solidification Cracking Under High-Speed Narrow Gap Welding with Tandem Torches, Quarterly Journal of the JWS, Vol.33, No.2 (2015), pp.190s-194s.

26) FARO Quantum ScanArm, https://www.faro.com/ja-jp/products/3d-manufacturing/faro-scanarm/, Accessed at Dec. 25, 2018.
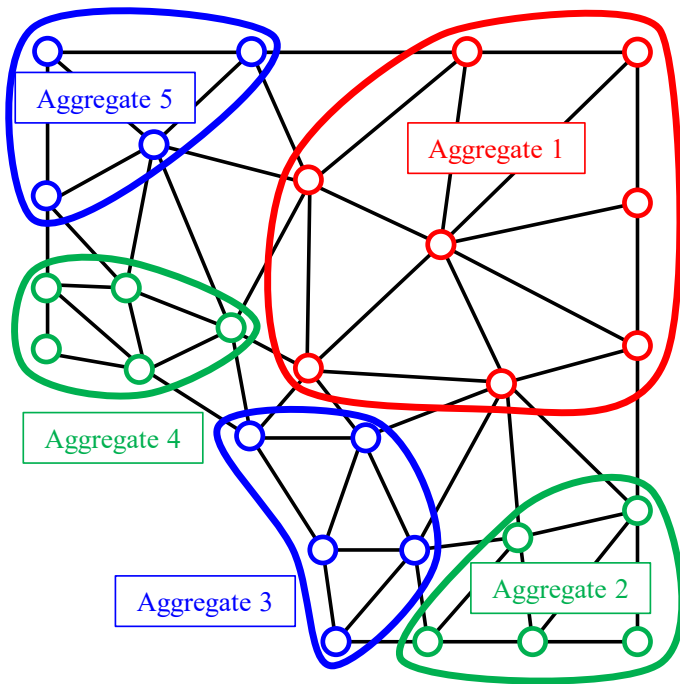
Figure 1. Typical 2D aggregates.

$$\{F_{\text{int}}\} = \sum_{e=1}^{Ne} \int_{V^e} [B]^T \{\sigma\} dV$$
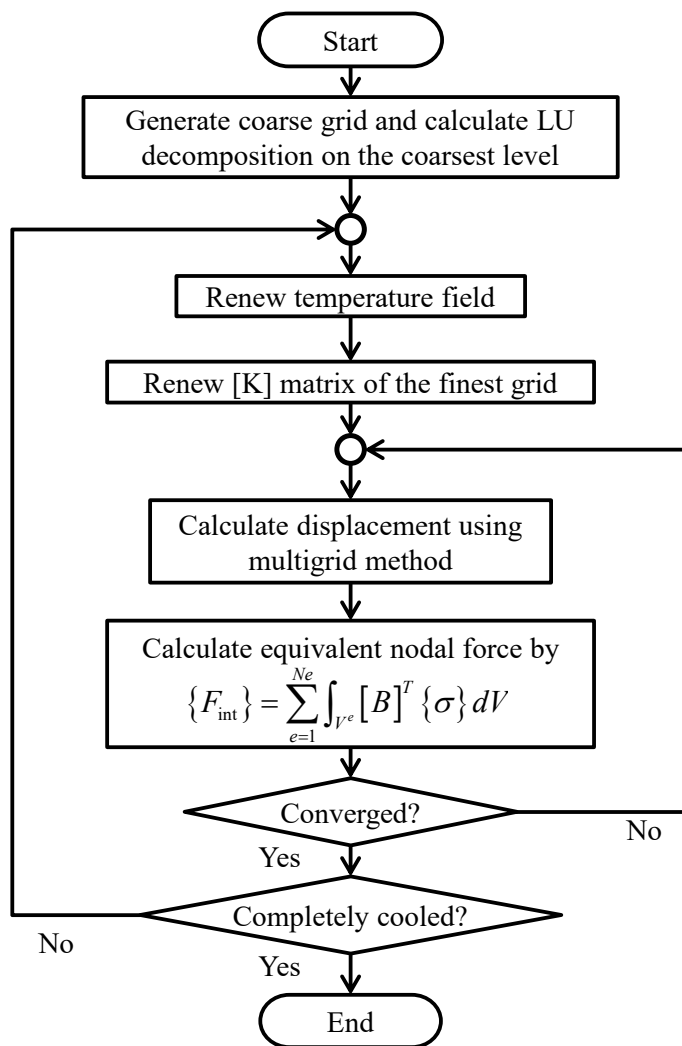
Figure 2. Flow of multigrid method introduced Idealized Explicit FEM.
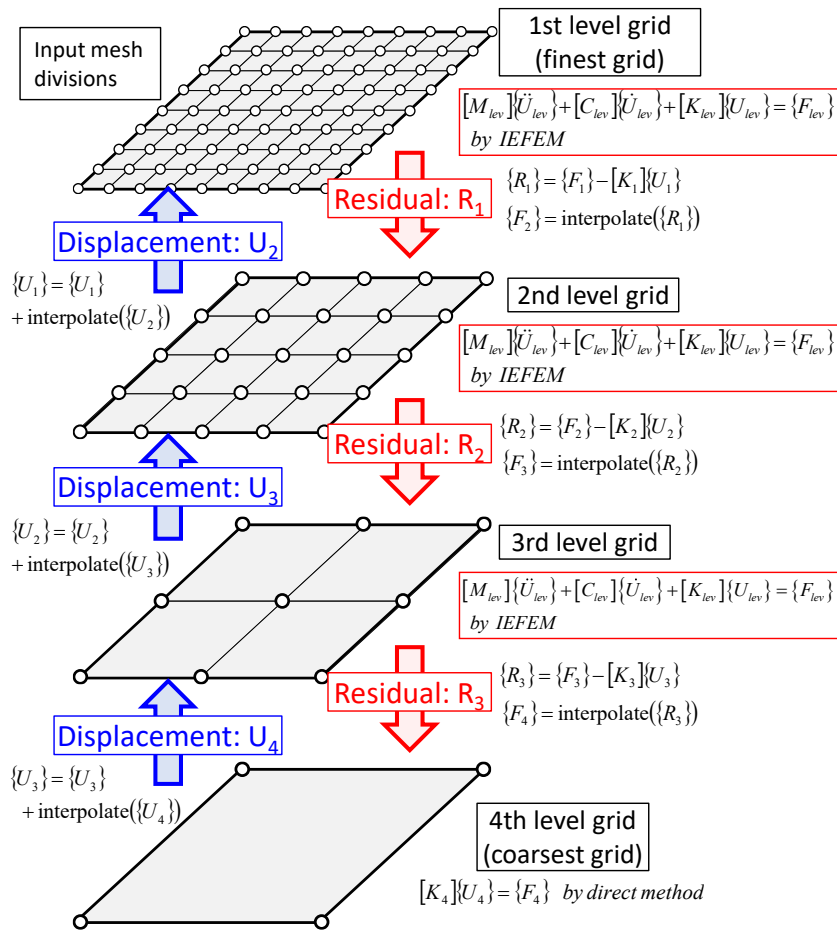
Figure 3. Schematic illustration of multigrid method introduced Idealized Explicit FEM.
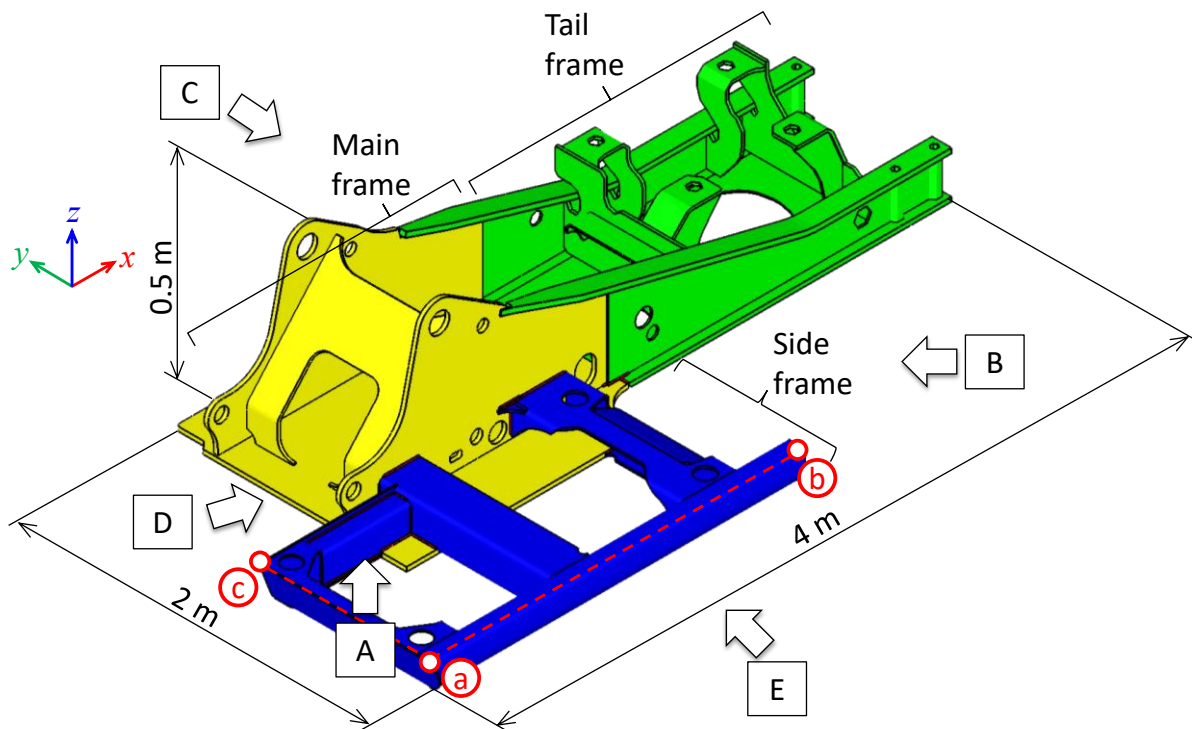
Figure 4. Analysis model of the base of construction machine.
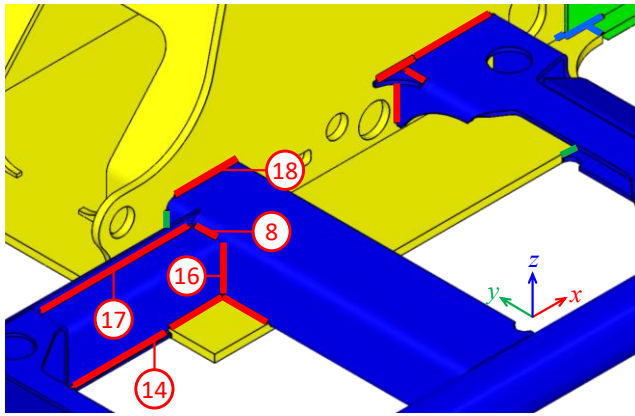
(a) View from point A.
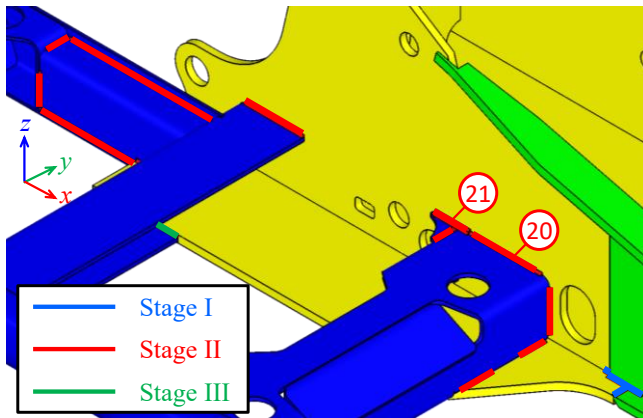
(b) View from point B.
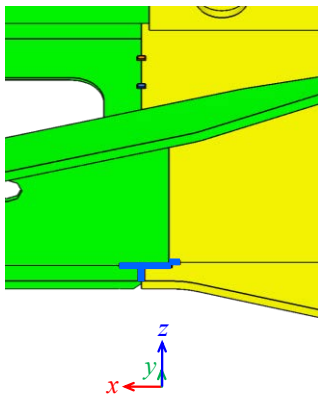
(c) View from point C.
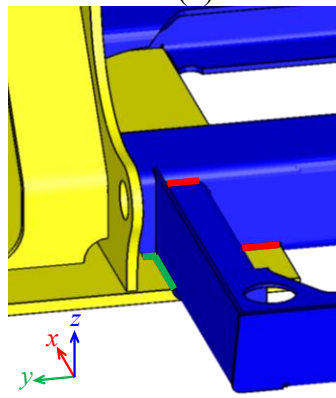
(d) View from point D.
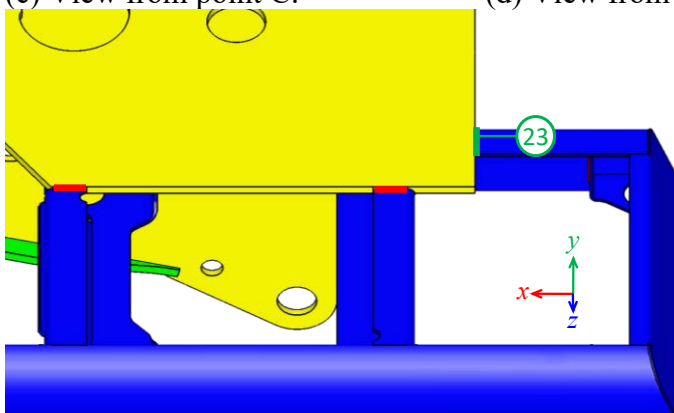
(d) View from point E.

Figure 5. Location of welding passes.

Table 1. Welding conditions.

Stage	Current (A)	Voltage (V)	Welding speed (mm/s)	Heat efficiency
I	293.0	24.0	4.5	0.8
II-1	260.0	24.5	5.0	0.8
II-2	245.0	26.0	3.7	0.8
II-3	290.0	24.5	6.0	0.8
III	293.0	24.0	4.5	0.8
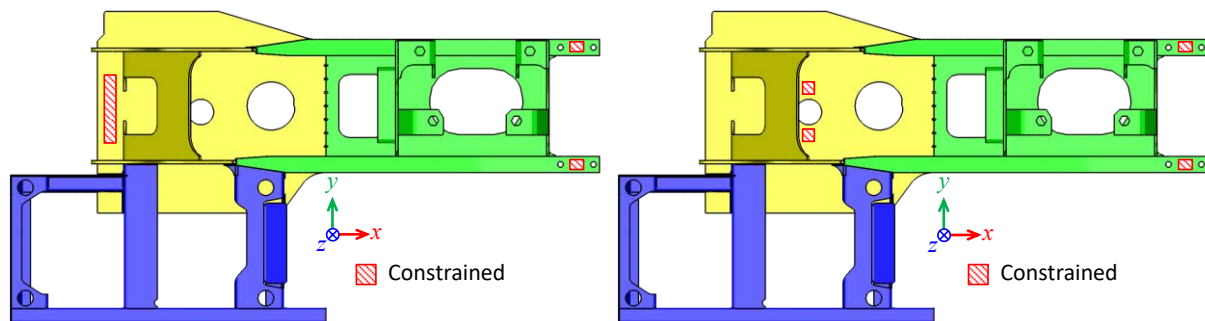
(a) 5-22 pass (stage II).

(b) 23-28 pass (stage III).

Figure 6. Constraint condition.
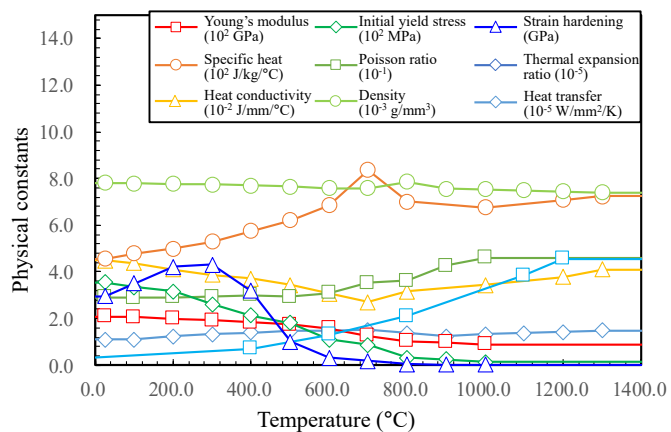
Figure 7. Temperature dependent material properties of SM490A.
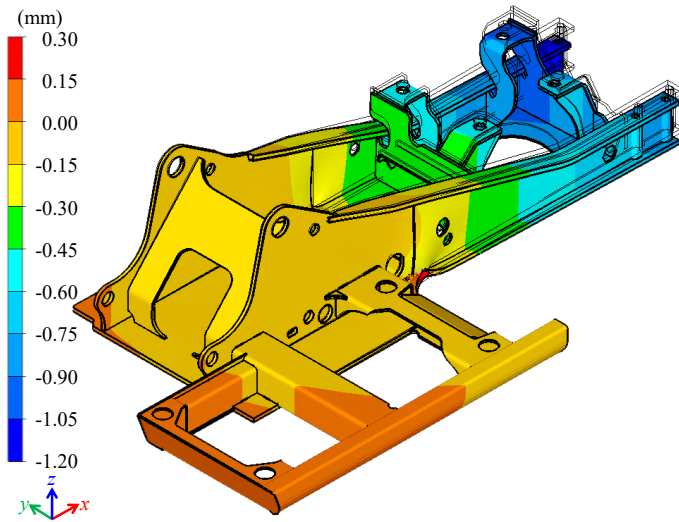
Figure 8. Distribution of displacement in z direction after the 4th welding pass.

(a) Before 14th pass.   (c) Before17th pass.
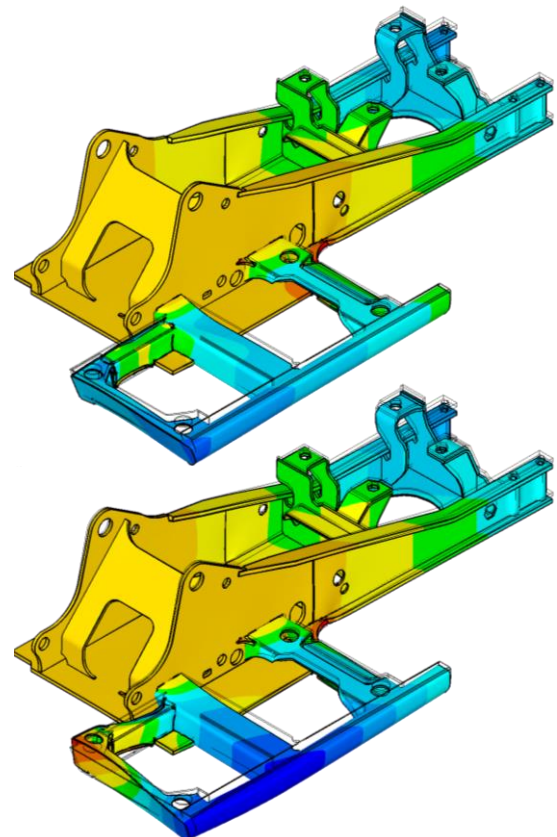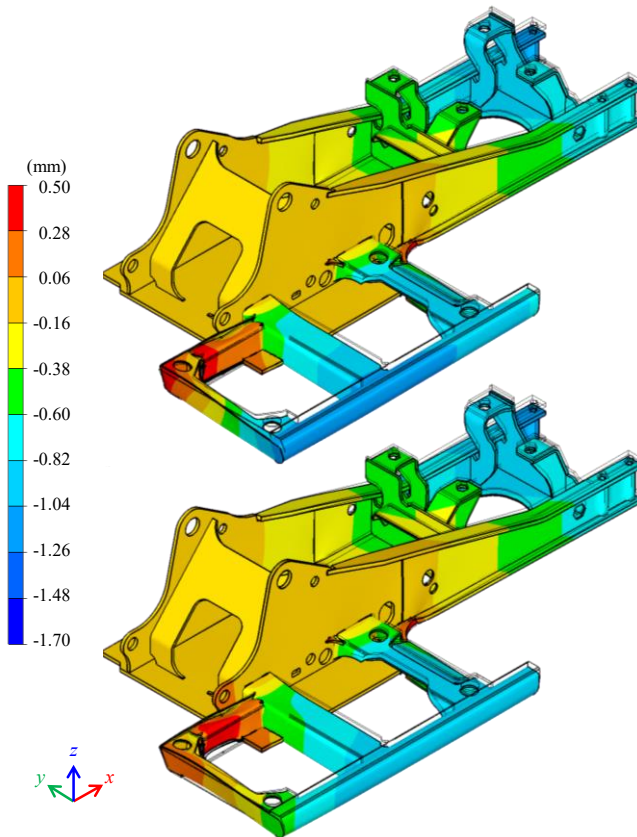
(b) After 14th pass.   (d) After 17th pass.

Figure 9. Change of displacement in z direction between before and after the 14th and 17th welding pass.
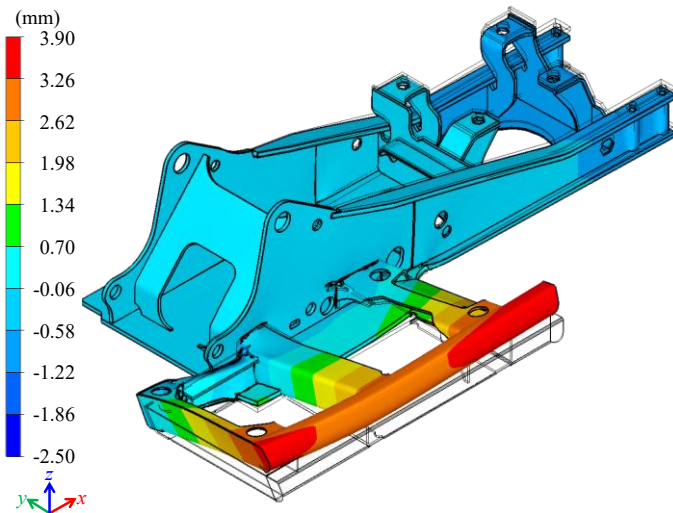
Figure 10. Distribution of displacement in z direction after the 22nd welding pass.
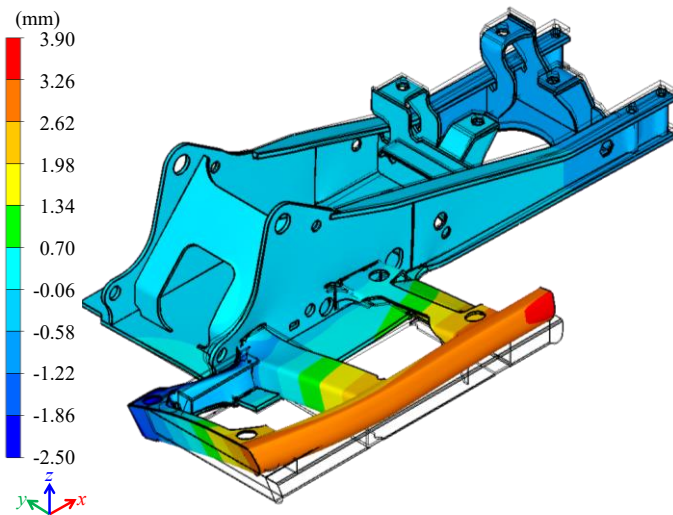
Figure 11. Distribution of displacement in z direction after all the welding passes.
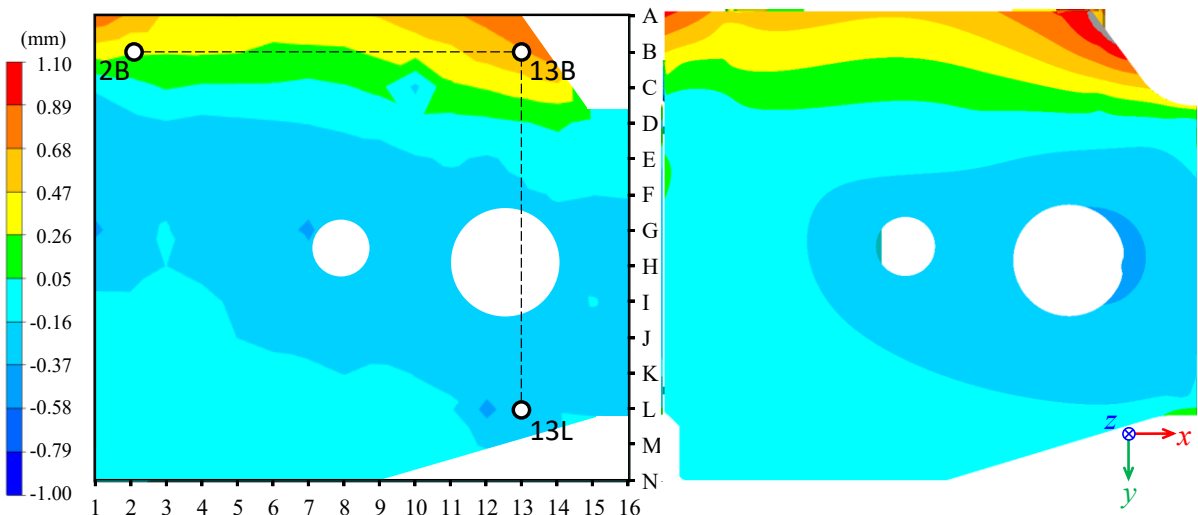
(a) Measured by FARO.   (b) Predicted by the proposed method.

Figure 12. Comparison of displacement in z direction on the base plate between

measurement and analysis.
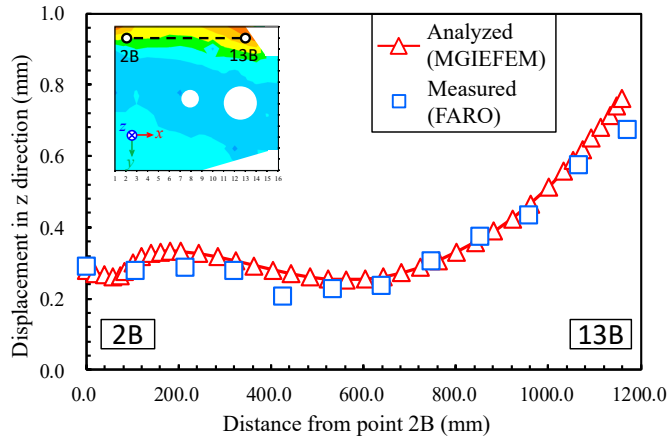
(a) Line 2B-13B.
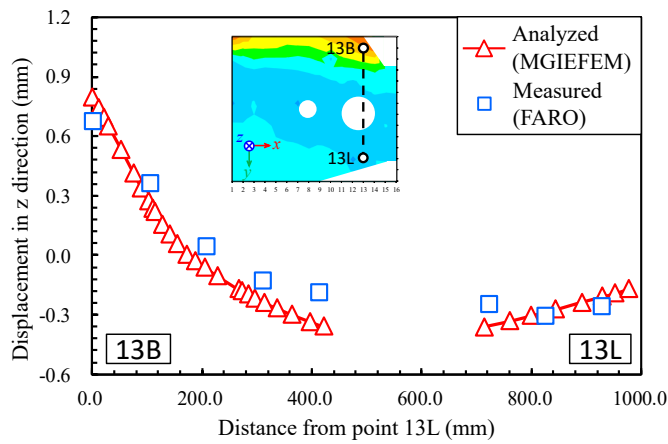
(b) Line 13b-13L.

Figure 13. Comparison of displacement in z direction on the base plate between measurement and analysis.

Table 2. Modified welding sequence according to transverse shrinkage.

Order	5	6	7	8	9	10	11	12	13	14	15	16	17	18	19	20	21	22
Pass no.	18	20	21	5	6	7	8	9	10	11	12	13	14	15	16	17	19	22
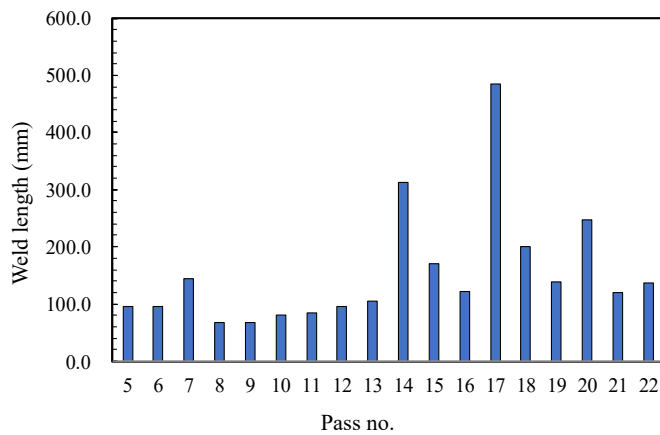
Figure 14. Weld length of each pass in robot welding.
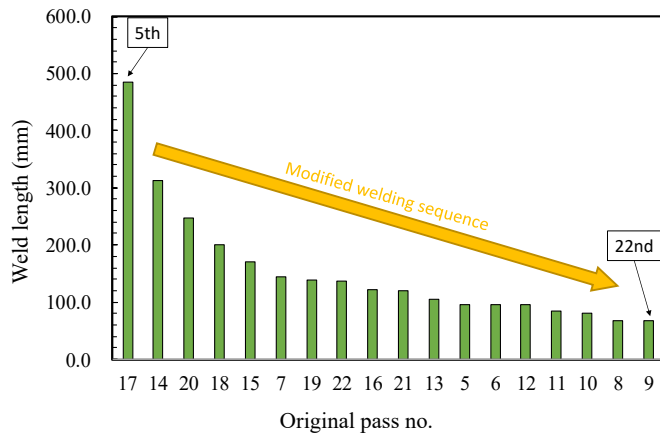
Figure 15. Modified welding sequence according to weld length.
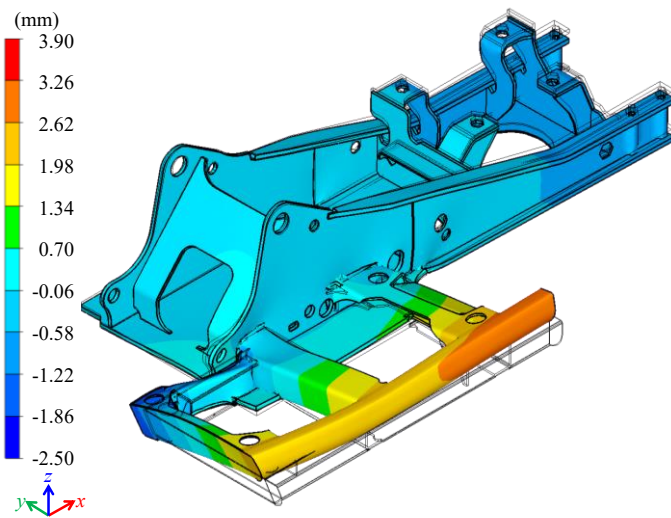
Figure 16. Predicted distribution of displacement in z direction using modified welding sequence according to transverse shrinkage.
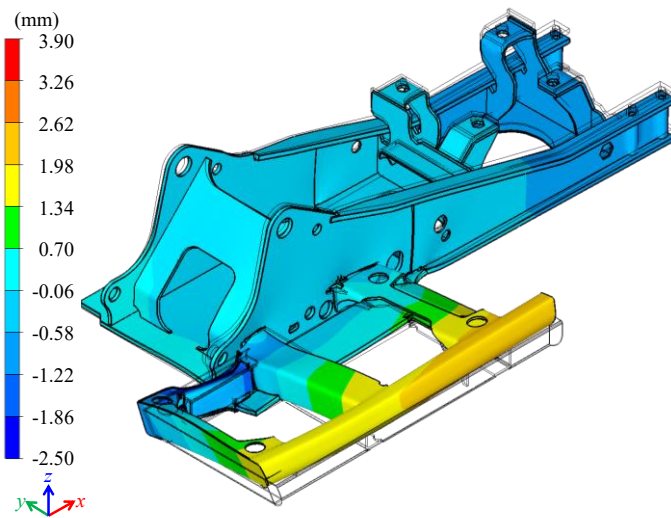
Figure 17. Predicted distribution of displacement in z direction using modified welding sequence according to weld length.
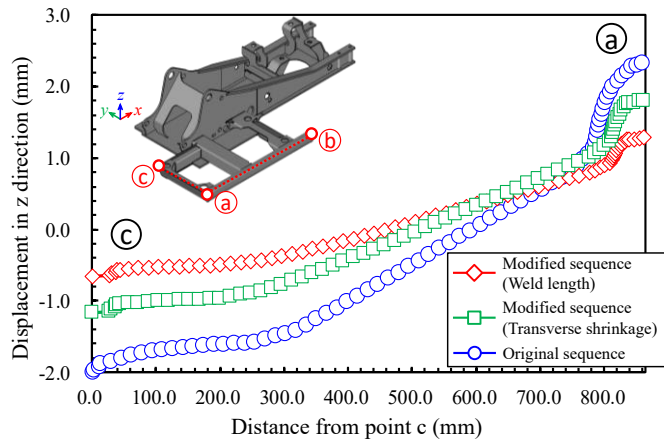
(a) Line c-a.
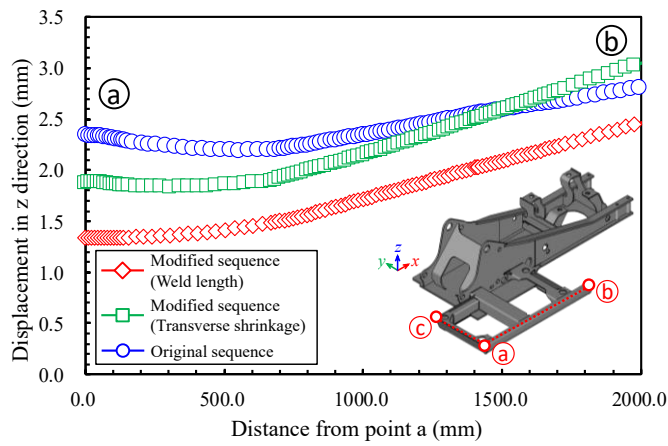
(b) Line a-b.

Figure 18. Comparison of displacement in z direction between original and modified welding sequence.